Measurements of void fraction, liquid temperature and velocity under boiling two-phase flows using thermal anemometry

Fabrice François, Henda Djeridi, Stéphane Barre, Michel Kledy

Version of Record: https://www.sciencedirect.com/science/article/pii/S0029549321003113
Manuscript_e91d2cecc82e7c8322518be90b6b13e9

Submitted to NED 2020

MEASUREMENTS OF VOID FRACTION, LIQUID TEMPERATURE AND VELOCITY UNDER BOILING TWO-PHASE FLOWS USING THERMAL-ANEMOMETRY

Fabrice FRANCOIS[1], Henda DJERIDI[2], Stéphane BARRE[2] , Michel Klédy
[1] CEA/DES/IRESNE/DTN/STCP/LTHC, 13115 Saint-Paul-Les-Durance FRANCE
[2] LEGI, 1209 Rue de La Piscine, 38610 Gières FRANCE
fabrice.francois@cea.fr; henda.djeridi@legi.grenoble-inp.fr; stephane.barre@legi.grenoble-inp.fr; michel.kledy123@hotmail.fr

ABSTRACT

Forced convective boiling is of great interest for several applications in the power and process industry, particularly in nuclear plants. Under certain nominal, incidental or accidental conditions, boiling crisis (considering Departure from Nucleate Boiling as well as Dry-Out) may lead to mechanical damage of the heated surface. An accurate prediction of the conditions leading to the occurrence of this phenomenon is then essential. It is believed that such an objective cannot be reached unless a good and accurate description of the associated two-phase flow is provided. In our work, we propose to use thermal anemometry for measuring the void fraction, the liquid temperature and liquid velocity for high pressure and high temperature Freon R134A boiling flow. Experiments have been conducted in a circular tube whose inner diameter and length are 19.2mm and 3.5m, respectively. The tube is heated by Joule effect. The sensor (hot-wire $d \sim 5\ \mu m$) has been operated with the Constant Current mode (CCA) and the multiple overheating method, which is classical for gas measurements but seems to be very innovative for liquid flows. This method, has been used to access simultaneously the liquid velocity and temperature. To consider for temperature effect on velocity calibration, a new non-dimensional representation of the calibration curve has been proposed. The frequency response of the probe has also been improved using a digital compensation method. The method has been first checked for single-phase flows and has shown that it was possible to get very accurate measurements of both mean and fluctuating liquid and temperature profiles. For boiling flows, a specific two-steps approach has been developed to first measure the void fraction where it is necessary to set a high overheat ratio leading to boiling on the wire surface and second to measure the liquid temperature and velocity for the case where boiling on the wire surface is not acceptable due to the multiple overheating method. An innovative method using probability density functions has been adapted from the pioneering work of Delhaye (1969).
Some tests have been conducted for boiling flows and the experimental results have been compared to previous ones using thermocouples and optical probes for respectively the liquid temperature and the void fraction. The experimental uncertainties have been carefully analyzed and they are estimated to be close to 0.5°C for the liquid temperature, ±2% for the void fraction (absolute uncertainty) and ±5% for the liquid velocity (relative velocity). Those data aim to be used for NEPTUNE_CFD code validation.

KEYWORDS
BOILING FLOWS, HOT WIRE, ANEMOMETRY, LIQUID VELOCITY, MULTIPLE OVERHEATS, VOID FRACTION

1 INTRODUCTION

Forced convective boiling is of great interest for several applications in the power and process industry, particularly in nuclear plants. Under certain nominal, incidental or accidental conditions, boiling crisis (Departure from Nucleate Boiling) may occur resulting in the meltdown of the heated surface. An accurate prediction of the conditions leading to the occurrence of this phenomenon is then essential. It is believed that such an objective cannot be reached unless a good and accurate description of the associated two-phase flow is provided. This work concerns the development of thermal anemometry for measuring the void fraction, the liquid temperature and liquid velocity under boiling flows. The paper is organized as following: the first part will be devoted to the presentation of the experimental device and the methodology which has been developed to use thermal anemometry within single phase flows. The second part of this article will focus on the boiling flows configuration and will detail the two-steps approach which has been specifically developed in order to measure the void fraction as well as the liquid velocity and temperature profiles. The experimental results will be presented and discussed in the third section. Finally, a conclusion will summarize the presented work and will identify some perspectives about the work that still needs to be performed in order to improve the quality of measurements.

2 EXPERIMENTAL SET-UP

2.1 Description of the experimental rig

As high-pressure steam-water experiments would be too expensive and difficult to achieve, Refrigerant R134A has been used as coolant fluid for simulating the operating conditions of a pressurized water reactor. Indeed, thanks to R134A's physical properties, it is possible to reproduce PWR's flow characteristics but for a much lower pressure, temperature and heat fluxes. The corresponding operating conditions are determined using five scaling criteria (Stevens and Kirby, 1964):

- Almost identical geometry (cross-section, heated area, cross-sectional area),
- Same vapor/liquid density ratio to scale the R134A system pressure P,

$$\left(\frac{\rho_f}{\rho_g}\right)_{R134A} = \left(\frac{\rho_f}{\rho_g}\right)_{water} \tag{1}$$

- Same Weber Number We to scale the R134A mass flux G,

$$\left(\frac{G^2 R}{\rho_f \sigma}\right)_{R134A} = \left(\frac{G^2 R}{\rho_f \sigma}\right)_{water} \tag{2}$$

- Same Boiling number Bo to calculate the corresponding heat flux q_p in R134A,

$$\left(\frac{q_p}{G h_{fg}}\right)_{R134A} = \left(\frac{q_p}{G h_{fg}}\right)_{water} \tag{3}$$

- Same inlet equilibrium quality $x_{eq,in}$to determine the R134A inlet temperature,

$$\left(x_{eq,in}\right)_{R134A} = \left(x_{eq,in}\right)_{Water} \Leftrightarrow \left(\frac{h_{l,in} - h_f}{h_{fg}}\right)_{R134A} = \left(\frac{h_{l,in} - h_f}{h_{fg}}\right)_{water} \tag{4}$$

Where ρ_f, ρ_g, σ, $h_{l,in}$, h_f, h_{fg}, q_p and R denote the saturated liquid density, the saturated vapor density, the interfacial tension, the inlet liquid enthalpy, the saturated liquid enthalpy, the latent heat, the heat flux and the radius of the pipe, respectively. These similarity criteria lead to the following flow characteristics for the R134A loop (see Table 1).

Control parameters	Water	R134A
Exit pressure [**MPa]**	10 to 16	1.4 to 2.6
Mass flux [**kg.m^{-2}.s^{-1}**]	500 to 5000	500 to 5000
Heat flux [**MW.m^{-2}**]	0.5 to 3	0.01 to 0.20
Inlet temperature [**°C**]	50 to 320	20 to 80
Equilibrium exit quality [-]	-0.3 to 0.5	-0.3 to 0.5
Re [-]	$5.10^4 - 10^6$	$5.10^4 - 10^6$

Table 1: Water operating conditions and corresponding R134A flow characteristics. Re is the Reynolds number defined as: $Re = GD_H/\mu$

DEBORA is a Freon R134A rig working within the ranges $0 - 4.5\ kg/s, 10 - 100°C, 1 - 41\ bar$ and $0 - 200\ kW$. Figure 1 gives a schematic of DEBORA. It is made of a pump, a pre-heater which imposes the temperature at the inlet of the test section, the test section whose description is given just after, a direct condenser and two heat exchangers which cool the liquid before it returns to the inlet of the pump. The circuit is pressurized by a thermal pressurizer. The test section (Figure 2) is a single vertical Stainless Steel (316 TI) tube with a circular cross section. The internal diameter is $d_{int} = 19.2\ mm$ and the external diameter is $d_{ext} = 21.2\ mm$. The length of the test section is $L_{ch} = 3.485\ m$ and it can be heated by Joule effect in whole or in parts, thanks to two power rectifiers who can deliver an electric current $I = 1250\ A$ at a voltage $U = 80\ V$. The test section is thermally insulated on its external face with a $6\ cm$ layer of rock wool, so that thermal power losses can be neglected. The test section boundary conditions are measured by using a Coriolis flowmeter for the mass flow rate, Platinum sensors for the inlet and the outlet temperature, pressure sensors for inlet and outlet pressure (pressure taps are located in the non-heated part of the tube *i.e.* $0.01\ m$ before and after the heated length), and an ammeter and Voltmeter for the electrical power. In addition, wall temperatures are measured by using three Platinum micro-probes (Pt 100, JUMO Platinum Temperature sensors) glued to the external face of the heated tube. They are located $0.02\ m$ before the end of the heated length and are distributed on a ring every 120°.
Local measurements into the fluid are performed at the outlet of the test section by using a device which is able to move the probe along one diameter (flow is assumed to be axisymmetric). The accuracy of positioning is $\pm 10\ \mu m$ and the moving resolution is close to $\pm 10\ \mu m$. Table 2 summarizes the uncertainties of the boundary conditions measurements.

	Sensor type	Uncertainty	Stability
Inlet temperature	Platinum sensor	$\pm 0.2°C$	$\pm 0.1°C$
Outlet temperature	Platinum sensor	$\pm 0.2°C$	$\pm 0.1°C$
Mass Flow Rate	Coriolis Flowmeter	$\pm 0.1\%$	$\pm 0.5\%$
Wall Temperature	Micro Platinum sensor (JUMO)	$\pm 0.6°C$	$\pm 0.1°C$
Pressure	Pressure sensor	$\pm 0.01\ bar$	$\pm 0.5\%$
Heat Power	Voltmeter/ammeter	$\pm 3\%$	$\pm 0.5\%$

Table 2: Experimental uncertainties for the boundary conditions

The stability of the thermal hydraulic conditions has been measured. The fluctuations of the control parameters of the loop have been registered during a seven hours test. The results are shown in Table 2. For example, we can notice that the fluctuation of the inlet temperature never exceed, in absolute value $\pm 0.1°C$.

2.2 Hot wire anemometry: Case of single-phase Flow

2.2.1 General principle

The principle of thermal anemometry consists on putting one or several sensors heated by Joule effect in an incident flow. The heated elements are then cooled by heat exchanges with the surrounding fluid. The resistance of the sensor is changed by the cooling through the flow. The change of the wire electrical resistance is then an indirect measurement of the velocity or the liquid temperature (Bruun, 1995)

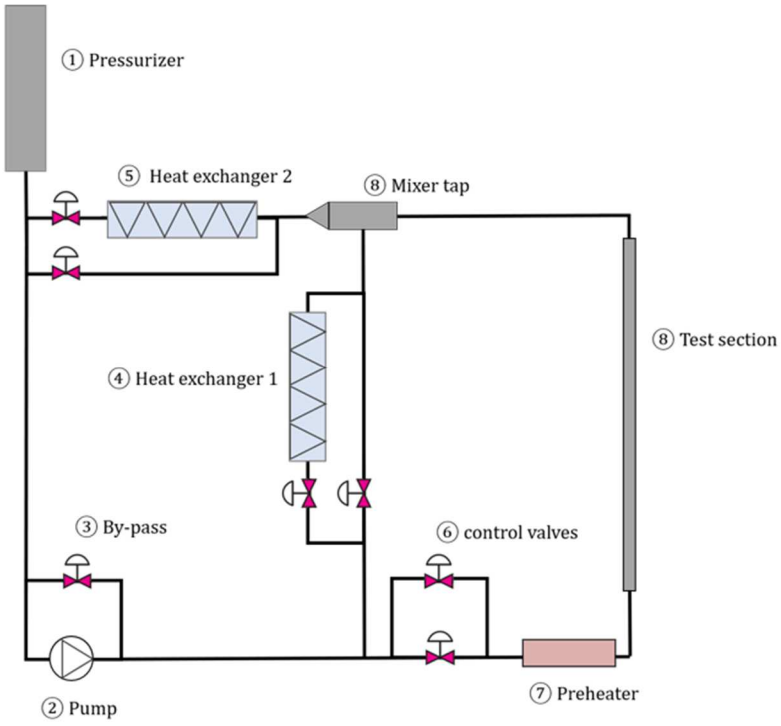

Figure 1: Schematic of DEBORA loop

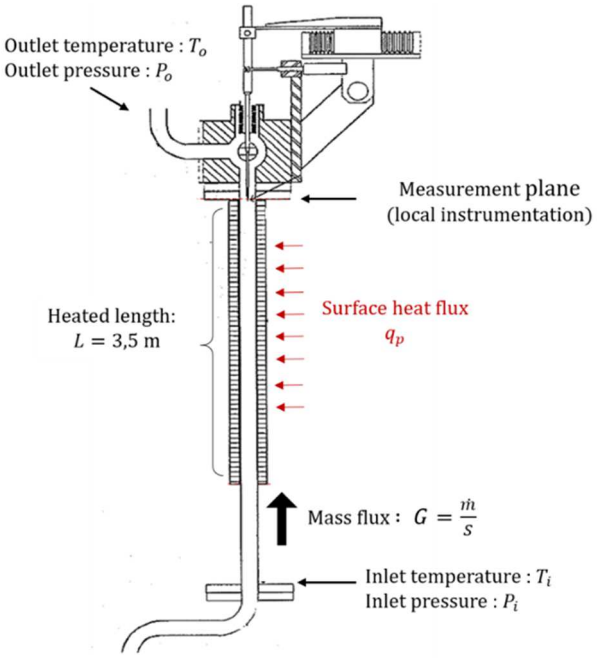

Figure 2: Description of the test section and the instrumentation moving system

When the thermal balance (steady state) is reached, the power produced by the Joule effect is completely evacuated by **convection** (equation 5):

$$R_w I^2 = h\pi dl(T_w - T_0) \tag{5}$$

Where T_w, R_w, I, T_0, h, d and l denote the equilibrium temperature and resistance of the sensor, the electrical current injected in the sensor, the fluid temperature, the heat exchange coefficient, the diameter of the probe and the length of the sensor, respectively. The electrical resistance of the sensor can be expressed as:

$$R_w = R_a[1 + \alpha_a(T_w - T_a)] \tag{6}$$

where T_a , R_a, T_w and α_a denote a reference temperature, the electrical resistance of the wire at temperature T_a and the coefficient of thermal sensitivity of the wire, respectively
By combining equations 5 and 6 and by introducing the Nusselt number$Nu_w \triangleq hd/\lambda$, the electrical resistance of the wire R_w can be expressed as:

$$R_w = \frac{R_0}{1 - \frac{\alpha_a R_a I^2}{Nu_{w,f}\pi l \lambda_f}} \Leftrightarrow R_w = R_0 + \frac{\alpha_a R_a}{Nu_{w,f}\pi l}\frac{R_w I^2}{\lambda_f} \tag{7}$$

Where the subscript f means that the thermophysical properties are evaluated at the film temperature (equation 10).

Thus, for low values of the electrical current I (cold wire mode), the resistance of the wire R_w is close to R_0 which means that the temperature of the wire is very close to the fluid temperature ($T_w \sim T_0$). On the other hand, for higher values of the current I, the temperature of the wire increases. The sensor operates in hot wire mode and the resistance R_w depends on both the temperature of the fluid T_0 and the velocity through the Nusselt number $Nu_{w,f}$. The operating temperature of the sensor can be characterized by the overheat ratio a_w defined as $a_w \triangleq (R_w - R_0)/R_0 = \alpha_a(T_w - T_0)$.

Sensors are thin metallic wires (Tungsten, Platinum, Platinum-Rhodium) with typical diameters of $d = 0.5 - 5\ \mu m$ and typical length of $l = 0.1 - 1\ mm$. For liquids, hot-films sensors (thin film deposited by sputtering on quartz support) are often used because of their robustness but they have bigger diameter ($d \sim 70\ \mu m$). In our study, since Freon R134A is an excellent electrical insulator, we used Tungsten wires with smaller diameters as $2.5\ \mu m$ and $5\ \mu m$ and a sensible length of $700\ \mu m$. Their smaller size is offering a better temporal and spatial measurement resolution compared to film probes. However, preliminary tests have shown that wire probes were chemically attacked by Freon R134A due to oxidizing nature of the Fluorine, but that film probes were not impaired. In order to be protected, the wire probes were coated with a layer of Sapphire deposited by Atomic Layer Deposition. The layer thickness was $20\ nm$. Results have confirmed that such a thickness is sufficient to get an effective protection.

2.2.2 Multiple overheating method

Due to its simplicity, we decided to operate the sensor in the constant current mode. Thus, and as shown by equation 7 , measuring both the liquid velocity and temperature requires at least two different sensors overheats: (i) a low current (cold wire mode) for temperature measurements (ii) a high current (hot-wire mode) for velocity measurements. In such an approach, velocity measurement is then impacted by the accuracy of the temperature measurements, when the

injected current is low. To overcome this limitation, the **multiple overheating method** was used. Originally developed by Corrsin (1947) this method has largely been used for measurement within single-phase gas flows. However, to our knowledge, this is the first time that this method is used in a liquid flow.
The multiple overheating method consists of successively injecting several currents into the wire for an imposed liquid velocity and temperature. For each value of the injected current, the equilibrium resistance of the wire R_w and the dissipated power $R_w I^2$ are measured.

According to equation 7, while assuming that the Nusselt number does not depend on the overheat ratio, the curve $R_w(R_w I^2)$ expected to be linear. R_0 is the intercept of the curves and only depends on the liquid temperature T_0 whereas the slope is a function of the Nusselt number, and therefore of the fluid velocity. By carrying out this procedure for several velocity/temperature samples, it becomes possible to calibrate the probe by connecting the fluid temperature T_0 to the wire recovery resistance R_0, and the Nusselt number $Nu_{w,f}$ to the incident velocity of the flow U and to the temperature of the liquid T_0. During the effective measurement process, this procedure will be reversed in order to obtain both the velocity and the temperature from the calibration curve defined by the equation 7.

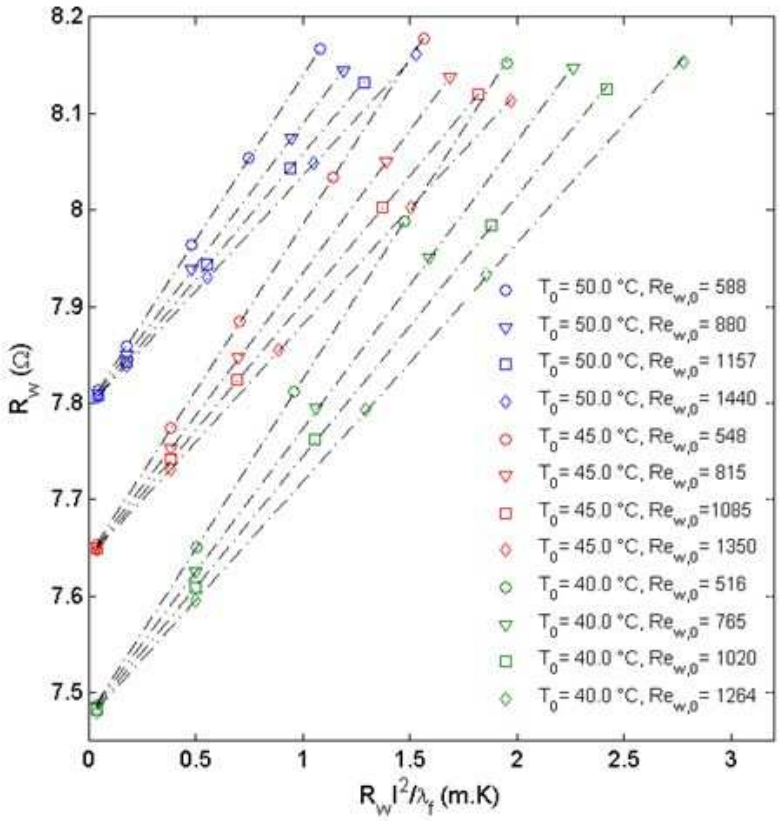

Figure 3. $R_w(R_w I^2)$ for several values of liquid temperature and velocity. The subscript "0" means that the thermophysical properties are evaluated at the liquid temperature. The subscript "f" means that the thermophysical properties are evaluated at the film temperature (see equation 10)

Figure 3 shows typical curves $R_w(R_w I^2)$ for several liquid temperatures T_0 and liquid velocities ($Re_{w,0} \triangleq \rho_L U d/\mu_L$). As expected those curves are linear. Duly, the recovery resistance R_0 (intercept of the curves) only depends on the fluid temperature but not on the fluid velocity. Nevertheless, the

Nusselt number, which corresponds to the slope of the curves, seems to be strongly influenced by the liquid temperature.

Calibration is performed within the test section under adiabatic conditions. For an imposed mass flowrate and liquid temperature T_0, we directly deduce the liquid temperature calibration curve $R_0(T_0)$ from Figure 3. The probe is located on the axis of the tube where the liquid velocity is calculated using the correlation of Zagarola and Smits (1998), whose accuracy is $\pm\ 0.55\%$, according to the authors. Once the velocity on the axis is known, the Nusselt number $Nu_{w,0}$ can be calculated and the calibration curve $Nu_{w,0}(Re_{w,0})$ can be obtained. Typical results are shown on Figure 4.

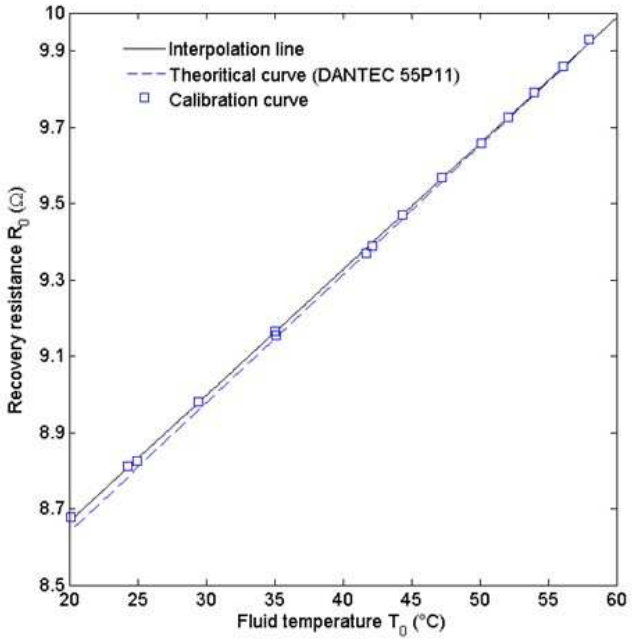

Figure 4 : Calibration curve for liquid temperature. Measurements were performed using a hot-wire probe $d = 5\ \mu m$

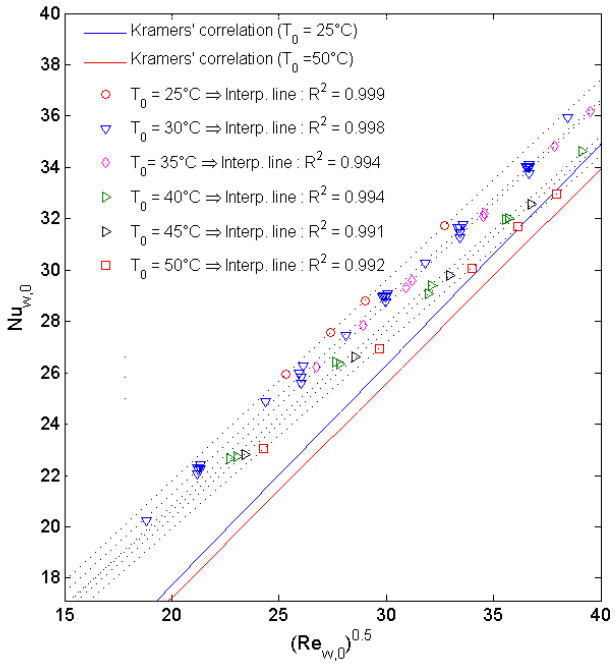

Figure 5 : Influence of the temperature on liquid velocity calibration curve. Measurements were performed using a hot-wire probe $d = 5\ \mu m$

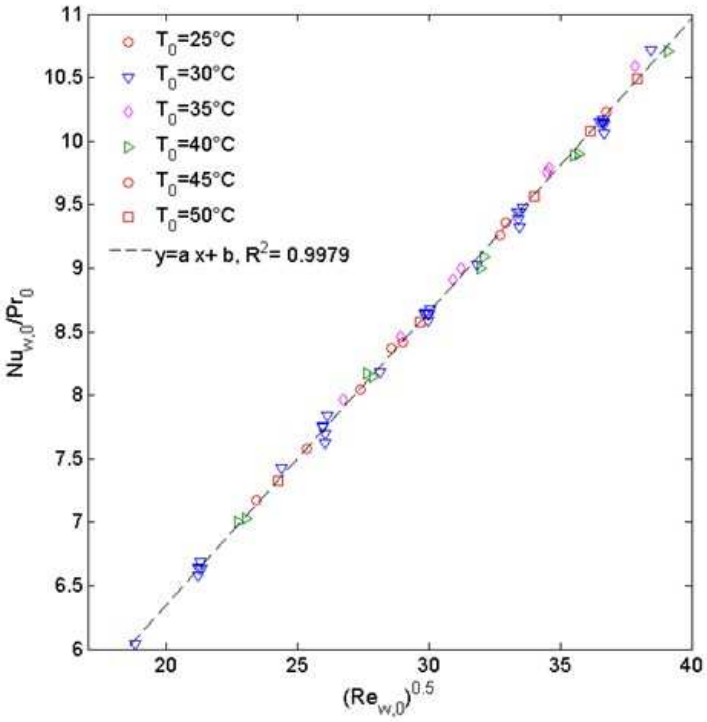

Figure 6: Calibration curve for the liquid velocity expressed in terms of $Nu_{w,0}/Pr_0$. Measurements were performed using a hot-wire probe $d = 5\ \mu m$

To overcome the influence of the liquid temperature on the velocity calibration curves (Figure 5), which would imply to use a different velocity calibration curve for each temperature, we replace the Nusselt number $Nu_{w,0}$ by $Nu_{w,0}/Pr_0$ where the Prandtl number is defined as $Pr \triangleq \mu C_p/\lambda$. Such

non-dimensional representation (Figure 6) allows to gather all the calibration data on a single linear curve whatever the liquid temperature. This **original approach** makes easier to consider the temperature effect on the velocity calibration process.

2.2.3 Frequency compensation procedure

To compensate the thermal inertia of the sensor and then improve the bandwidth of the anemometer (which is of a great importance for measuring the fluctuating quantities), we use a method of digital signal processing which makes possible to compensate *a posteriori* for the sensor filtering effect. Widely described by Tagawa *et al.* (1998) or Arwatz *et al.* (2013)), the method simply consists of applying an amplifying filter to the experimentally measured voltage. This amplifying filter has its cutoff frequency equal to the theoretical cutoff frequency of the anemometer f_C but with an opposite.

According to Comte-Bellot (1976), the theoretical cut-off frequency can be expressed as:

$$f_c \triangleq 1/2\pi\tau_c = \frac{2Nu_{w,f}\lambda_f}{\pi d^2 c_{pw}\rho_w(1+a_w)} \tag{8}$$

where c_{pw} and ρ_w are the specific heat capacity and the density of the wire. An order of magnitude of the cut-off frequency can be calculated.

The Nusselt number of the wire can be given for example by the correlation of Kramers (1946):

$$Nu_{w,f} = 0.42\ Pr_f^{0.2} + 0.57 Pr_f^{0.33}\sqrt{Re_{w,f}} \tag{9}$$

Where the subscript f means that the physical properties are evaluated at the film temperature defined by:

$$T_f = \frac{T_w + T_0}{2} \tag{10}$$

T_0 is the liquid temperature whereas T_w is the wire temperature.
We consider the following thermal hydraulic conditions:

- Flow velocity $2\ m/s$
- Liquid temperature $T_0 = 20\ °C$
- Pressure $P_s = 14\ bar$
- Overheat ratio $a_w = 0.1$
- Tungsten wire : diameter 5 µm

Under such conditions, the theoretical cutoff frequency given by equation 9 is close to 105 Hz. This frequency must be compared to the highest frequency that may be encountered in the in the flow. According to Albrecht *et al.* (2003), the expected highest frequency in the flow is given by :

$$f_{max,f} = \frac{\bar{u}}{2\pi L} Re^{3/4} \tag{11}$$

Where $\bar{u}$ depicts a characteristic mean velocity that we choose to be equal to the mean axial velocity at the tube exit and L a macro length scale that we choose to be the tube diameter. Re is the Reynolds number whose order of magnitude is, according to thermal hydraulic conditions given previously close to 5.10^5.

We obtain a maximum frequency whose order of magnitude is close to 200 kHz. Thus, strictly speaking from a theoretical point of view, it should be necessary to implement a frequency compensation process for the hot-wire signal in order to be able to correctly characterize the structure of the turbulent field. Nevertheless we can show that this has only a weak influence on the quality of the measurements.

According to Charonko and Prestridge (2017) or Pope (2000), orders of magnitude of the Taylor and Kolmogorov micro-scales of the flow, λ_T and η_K respectively, are given by:

$$\lambda_T = \sqrt{10}\,.d\,.Re^{-1/2} \tag{12}$$

And

$$\eta_K = d.Re^{-1/4} \tag{13}$$

For thermal hydraulic conditions given above, those scales are estimated to $\lambda_T \sim 100\,\mu m$ and $\eta_K \sim 2\,\mu m$ respectively. The order of magnitude of the full-scale is given by the radius of the pipe ($R \sim 10\,mm$). According to the diameters of our probes, namely 2.5 and 5 µm, we therefore conclude that we should be able to characterize structures whose characteristic length is greater than the Taylor micro-scale, provided frequency bandwidth is wide enough. However, this point needs to be checked since most of the turbulent kinetic energy will be dissipated at the lowest frequencies corresponding to the integral scale.

In Figure 7, we plotted the power spectral density for different values of the cutoff frequency (from 500 Hz to 5 kHz). The considered flow is an adiabatic single-phase liquid flow whose working conditions are:

- Pressure: $P_s = 26$ bar,
- Mass velocity $G = 1000\ kg.m^{-2}s^{-1}$
- Liquid temperature $T_0 = 19.9C$
- Probe radial position $r^* = 0.8$
- Overheat ratio $a_w = 0.18$

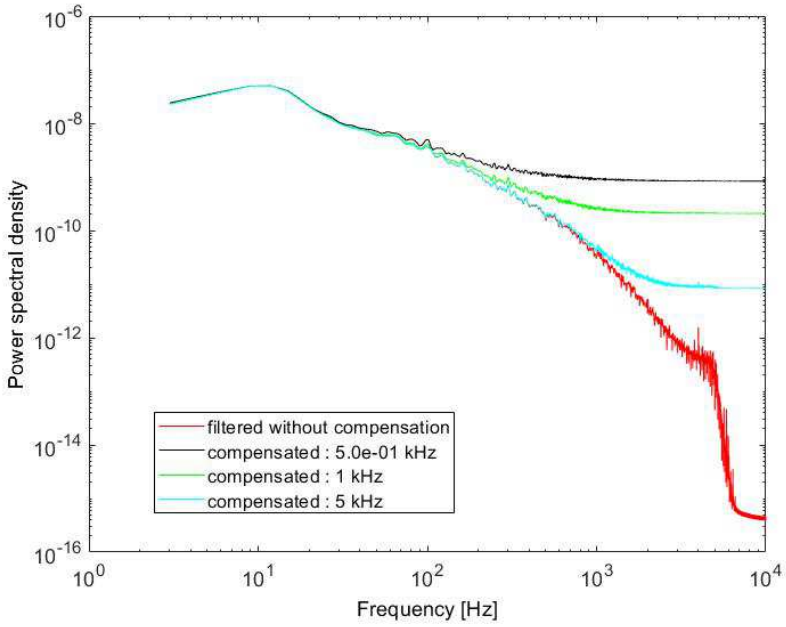

Figure 7: Power spectral density with and without frequency compensation $P_s = 26\ bar$

- $G = 1000\ kg.m^{-2}s^{-1}$ - $T_0 = 19.9\ °C$ - $r^* = 0.8$ - a_w= 0.18

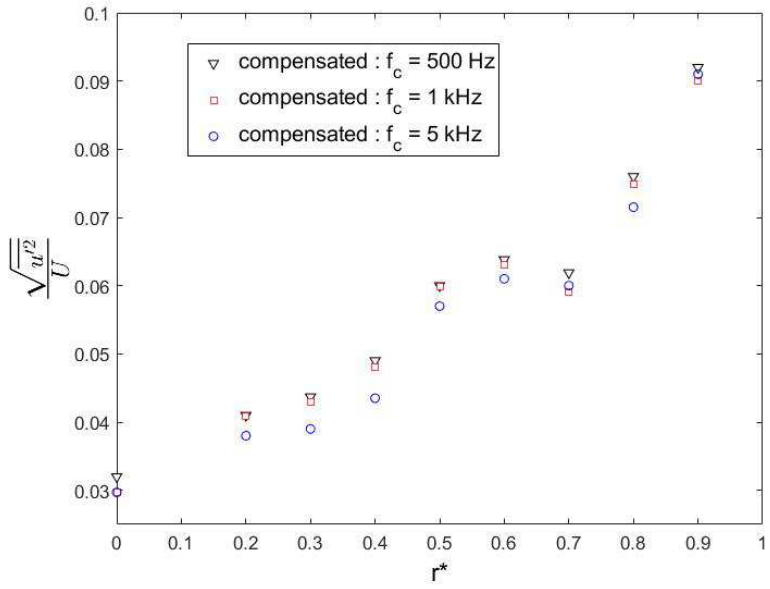

Figure 8 : Turbulent fluctuations of the velocity $P_s = 26\ bar$ - $G = 1000\ kg.m^{-2}s^{-1}$ - $T_0 = 19.9\ °C$ - a_w= 0.18

We can see that the hot wire compensation frequency process has only a weak influence on the calculated power spectral density. Using the procedure described in the next section (2.2.4), we also plotted on Figure 8 the turbulent fluctuations of the liquid velocity for different values of the compensation frequency. It can be seen that the measured turbulence rate seems to be very weakly influenced by any change of the hot-wire compensation frequency. This indicates that most of the turbulent kinetic energy do correspond to flow structures associated to frequencies lower than 500 Hz. This behavior was expected since the frequency corresponding to the integral scale of the flow (that canbe obtained by dividing the flow flow velocity by the pipe radius) is about 250 Hz. It is therefore normal that we no longer measure a lot of energy for frequencies greater than 500 Hz.

2.2.4 Procedure for measuring turbulent quantities

In order to measure the turbulent fluctuations of velocity and temperature, we use the fluctuation diagram method. The method consists of expressing the fluctuation of the instantaneous sensor voltage e'_w as a function of the fluctuation of the liquid velocity u' and the liquid temperature T' as:

$$\frac{e'_w}{e_w} = F\frac{u'}{U_L} + G\frac{T'}{T_L} \tag{14}$$

Where $F \triangleq \partial \ln(e_w)/\partial \ln(U_L)$ and $G \triangleq \partial \ln(e_w)/\partial \ln(T_L)$ are velocity and temperature sensitivity coefficients. Since the Nusselt number Nu_w varies linearly with the square root of the Reynolds number Re_w as shown in section 2.2.2, the expressions for the sensitivity coefficients F and G can be simplified as:

$$F = 0.5\ \frac{a_w}{1+a_w}\ ;\ G = -\alpha_0 T_w + \frac{a_w}{1+a_w}\left(1 + n - \frac{m}{2} + \frac{k}{2}\right) \tag{15}$$

Where the coefficients n, m, k only depend on the fluid thermophysical properties and are defined as:

$$n = \frac{\partial \ln(\mu)}{\partial \ln(T_L)}, m = \frac{\partial \ln(\lambda)}{\partial \ln(T_L)}, k = \frac{\partial \ln(\rho)}{\partial \ln(T_L)} \tag{16}$$

For calculation details, the reader should refer to Corrsin (1947) and Morkovin (1956).
It is possible to deduce from equation (8) the equation of the so-called fluctuations diagram by squaring, time-averaging and finally dividing equation (8) by G^2 after combining with equations (9) and (10):

$$\sqrt{\mathcal{H}(\mathcal{R})} = \frac{\sqrt{\overline{e_w'^2}}}{\overline{e_w} G} = \left[\mathcal{R}^2 \left(\frac{\overline{u'^2}}{\overline{U_L^2}} \right) + 2\mathcal{R} \frac{\sqrt{\overline{u'^2}}}{\overline{U_L}} \frac{\sqrt{\overline{T'^2}}}{\overline{T_L}} \mathcal{R}_{U,T} + \left(\frac{\overline{T'^2}}{\overline{T_L^2}} \right) \right]^{0.5} \tag{17}$$

Where $\mathcal{R}_{U,T}$ and $\mathcal{R}$ are defined as $\mathcal{R}_{U,T} \triangleq \frac{\overline{u'T'}}{\sqrt{(\overline{u'^2 t'^2})}}$ and $\mathcal{R} \triangleq -\frac{F}{G}$ respectively.

Equation 17 is a parabolic equation whose coefficients are directly linked to the fluctuating quantities that are under investigation. The experimental procedure then consists of varying the coefficient $\mathcal{R}$ by injecting several currents into the sensor to obtain the experimental curve $\mathcal{H}(\mathcal{R})$. Then, by using the least squares regression method, we can determine the fitting coefficients of the parabola (equation 17) and deduce the variances of the velocity and temperature fluctuations $\overline{u'^2}$ and $\overline{T'^2}$ as well as their correlation $\overline{u'T'}$. It can be noticed that the temperature fluctuations $\overline{T'^2}$ are given by the intercept of the diagram and the velocity fluctuations are given by the slope of the asymptote. As a result, the measurement accuracy of the temperature fluctuations is greatly affected by the signal-to-noise ratio of the hot wire at low overheating whereas the accuracy of the velocity fluctuations measurements depends on the correct determination of the asymptotic slope which requires to operate at high overheat ratios.

2.3 Hot wire-anemometry: Case of boiling flow

In case of boiling flow, the main problem is to determine the Phase Indicator Function (PIF). As the heat transfer coefficient between the sensor and the surrounding fluid is lower when vapor is in contact with the probe, the temperature of the sensor increases and so does the wire voltage, resulting in a voltage peak, whose level is distinct from the voltage fluctuations due to the turbulence. The higher overheat ratio a_w, the more marked is such behavior. Then, classically, a threshold method applied on the raw signal or on its derivatives leads to a correct phasic discrimination. This method has been widely used for adiabatic flows (Liu and Bankoff (1991); Farrar *et al.* (1995)).

Unfortunately, some preliminary tests have shown (Figure 9 to Figure 12) that similar results for Freon R134A would require overheat ratio leading to boiling occurrence over the sensor surface. Indeed, when the overheat ratio is too weak, the voltage peaks corresponding to vapor bubbles passing over the sensor are too low and they can't be distinguished from the voltage changes resulting from the velocity and temperature fluctuations or from the noise. So, it appears that in order to properly identify the phase which is in contact with the sensor, it is necessary to allow boiling on the sensor's surface. Dix (1971), who performed void fraction measurements using anemometry in Freon R113 boiling flows already mentioned this result and indicated that such operating conditions were acceptable for determining the void fraction, despite the boiling occurrence on the surface of the sensor. However, according to the methodology presented in section 2.2, it is not possible to measure the liquid velocity under boiling conditions on the surface of the sensor because the method is based upon the assumption of a single-phase convective heat transfer between the sensor and the surrounding fluid.

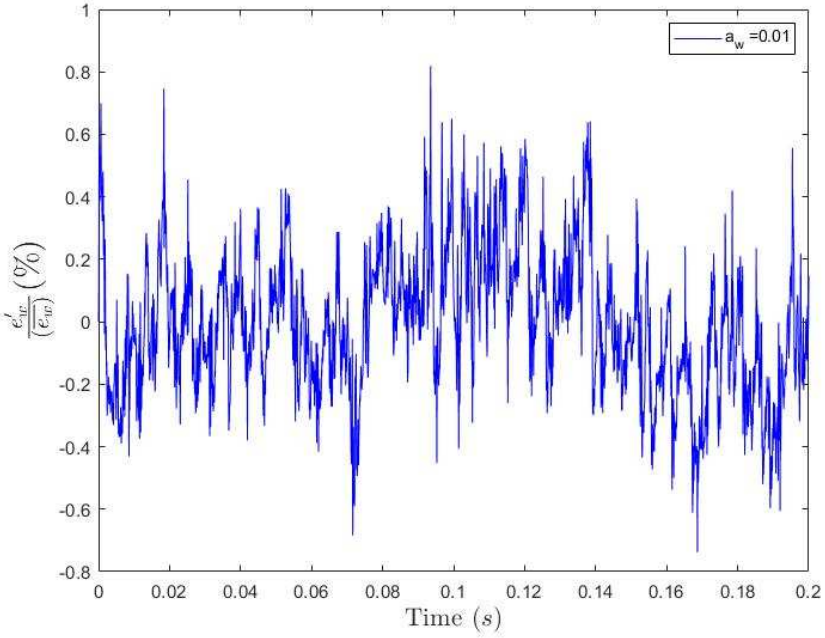

Figure 9: Fluctuations of the normalized voltage of the sensor ($e'_w/\overline{e_w}$) $a_w = 0.01$. Boiling occurs at $a_w \geq 0.04$. Void fraction $\alpha = 4\%$

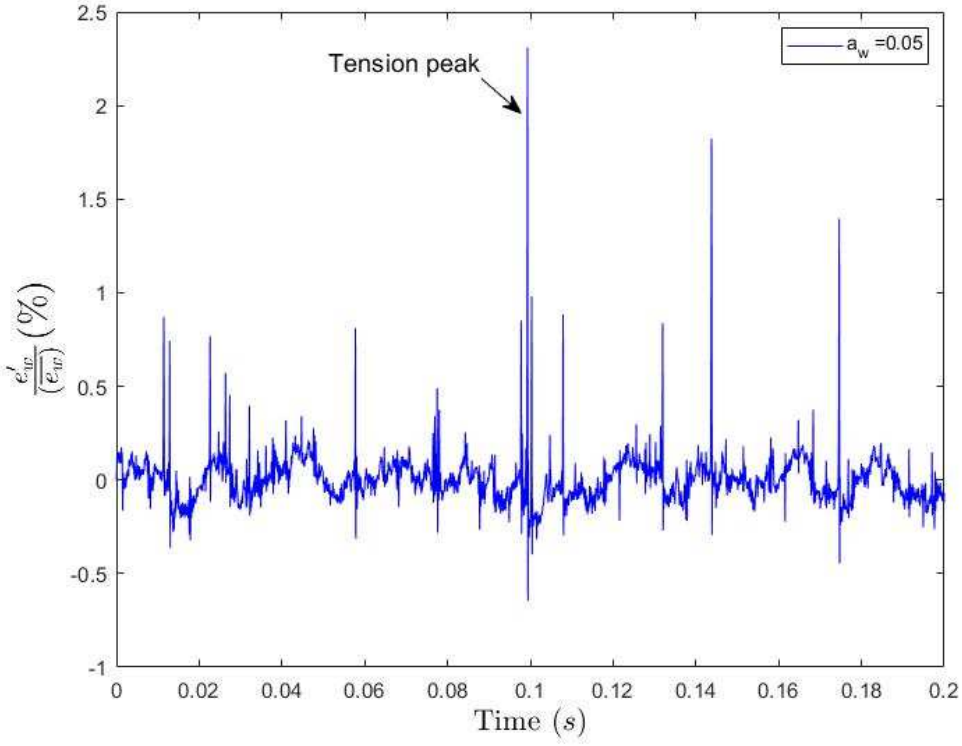

Figure 10: Fluctuations of the normalized voltage of the sensor ($e'_w/\overline{e_w}$) $a_w = 0.05$. Boiling occurs at $a_w \geq 0.04$. Void fraction $\alpha = 4\%$

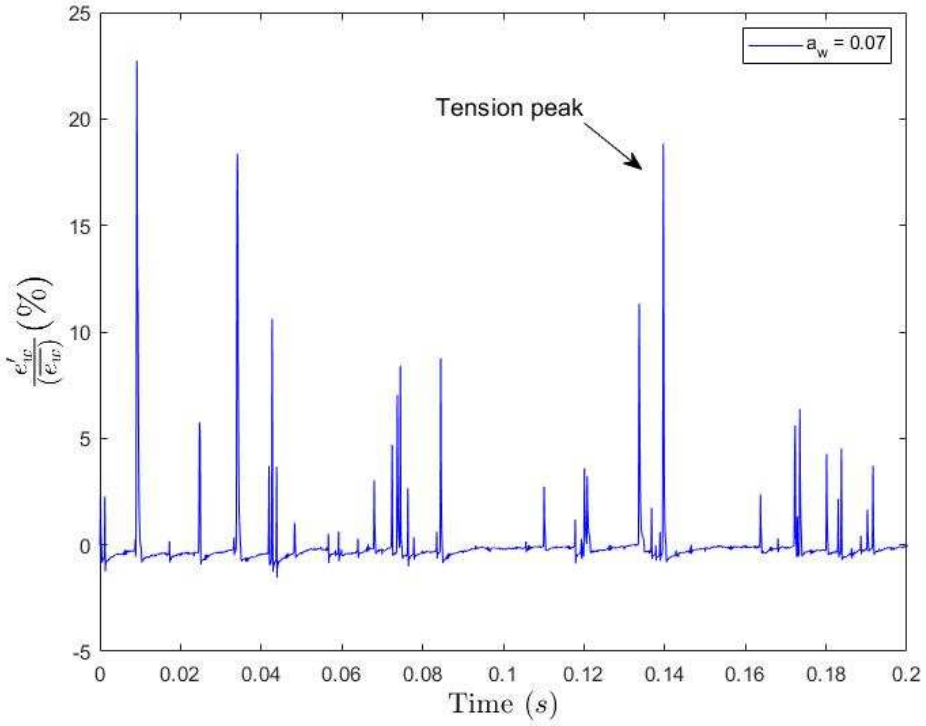

Figure 11: Fluctuations of the normalized voltage of the sensor ($e'_w/\overline{e_w}$) $a_w = 0.07$. Boiling occurs at $a_w \geq 0.04$. Void fraction $\alpha = 4\%$

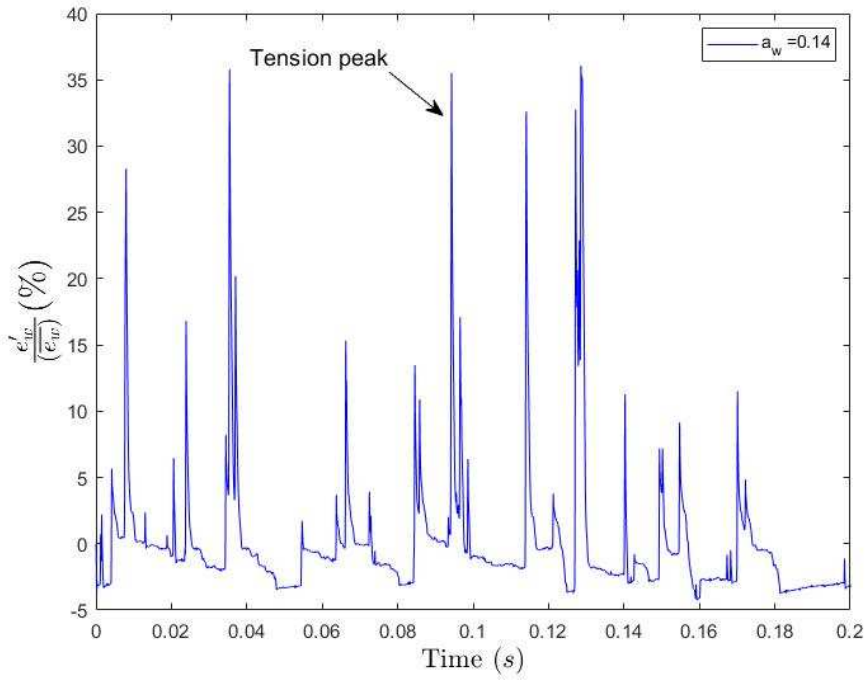

Figure 12: Fluctuations of the normalized voltage of the sensor ($e'_w/\overline{e_w}$) $a_w = 0.14$. Boiling occurs at $a_w \geq 0.04$. Void fraction $\alpha = 4\%$

As a consequence, we propose a two-steps approach to perform the measurements under boiling conditions: (i) a first step devoted to void fraction measurements and where boiling over the

sensor's surface will be allowed and (ii) a second step devoted to the determination of both the liquid velocity and temperature with no boiling occurrence on the sensor's surface. However, as it will be explained later, this second step will require the knowledge of the void fraction. Both steps are then complementary.

2.3.1 Void fraction determination

As explained before, the method for void fraction measurement is based upon a thresholding of the voltage signal. First the raw signal is filtered with a band pass filter whose cutoff frequencies are $f = 50\ Hz$ and $f = 10\ kHz$ to eliminate both low-frequency voltage fluctuations below 50 Hz and high frequency noise above 10 kHz (a complete description of the experimental set-up is given in the Appendix). Then the derivative of the signal is calculated and numerically amplified to get a better contrast between both phases. Finally, two thresholds (low and high levels) are applied to the resulting signal in order determine the PIF. Those two thresholds are expressed as $s_L = \delta \times \max(|e_w|)$ and $s_L = \delta \times \min(|e_w|)$ respectively so that their influence can be studied by only varying the parameter δ.

Once the PIF is determined, the void fraction can be obtained by time-averaging the PIF. The parameter δ has been determined by comparing the void fraction measured by anemometry and the void fraction measured using an optical probe for a given test. Despite the optical probe cannot be considered as a perfect measurement instrument, we will consider in this study that the void fraction measured with optical probe is a baseline measurement since, according to Garnier *et al.* (2001), the absolute uncertainty for the void fraction measurement by using an optical is $\pm 2\%$. One should note that Garnier *et al.* (2001) performed measurements with optical probes in very similar operating conditions to the current ones.

Figure 13 and Figure 14 show the results of this analysis. On Figure 13, the value of δ is determined by using anemometry to get the same local void fraction than the one measured by the optical probe for a given radial location $r^* = 0.8$. The optimum value seems to be $\delta = 0.01\%$.

We plotted on Figure 14 the results of a sensitivity analysis to study the impact of the parameter δ on the whole radial void fraction profile determination. We can notice that this value of δ leads to the best reconstruction of the void fraction profile, despite its value has only been determined for one particular void fraction. If we consider a higher value, we underestimate the void fraction whereas that is the contrary for too low values of this parameter. Consequently, this value will be retained for all the future tests.

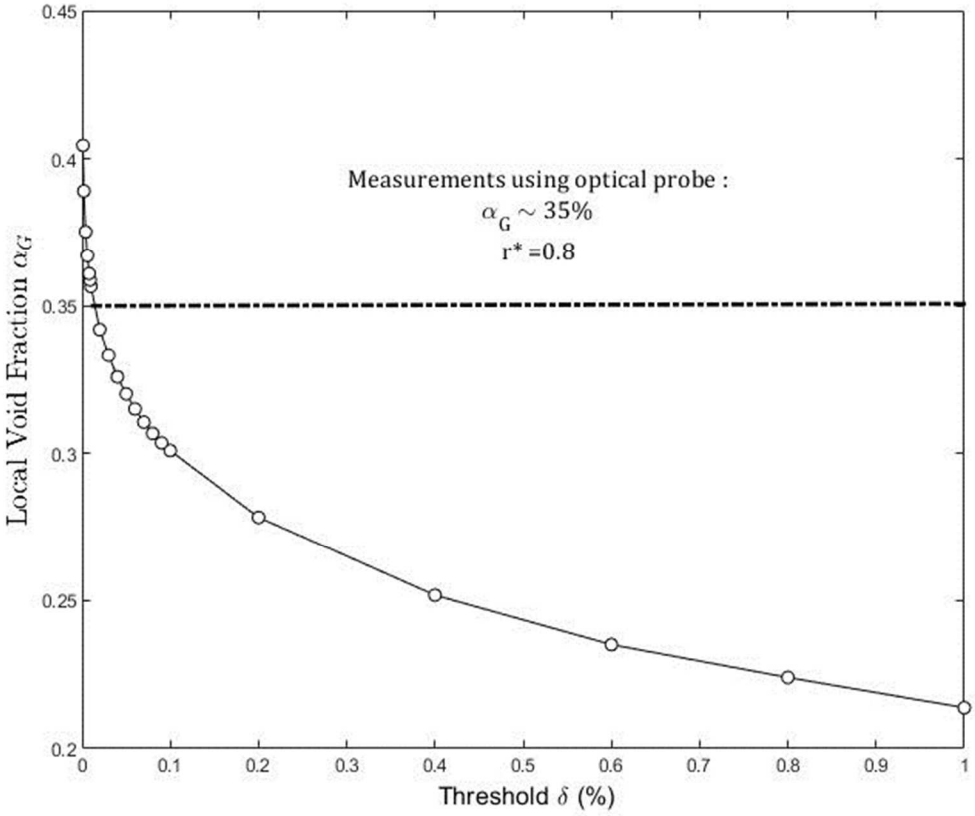

Figure 13: the best value of δ is determined for void fraction measured at $r^* = r/R = 0.8$ Measurements have been performed with a Tungsten wire probe $d = 5\ \mu m$

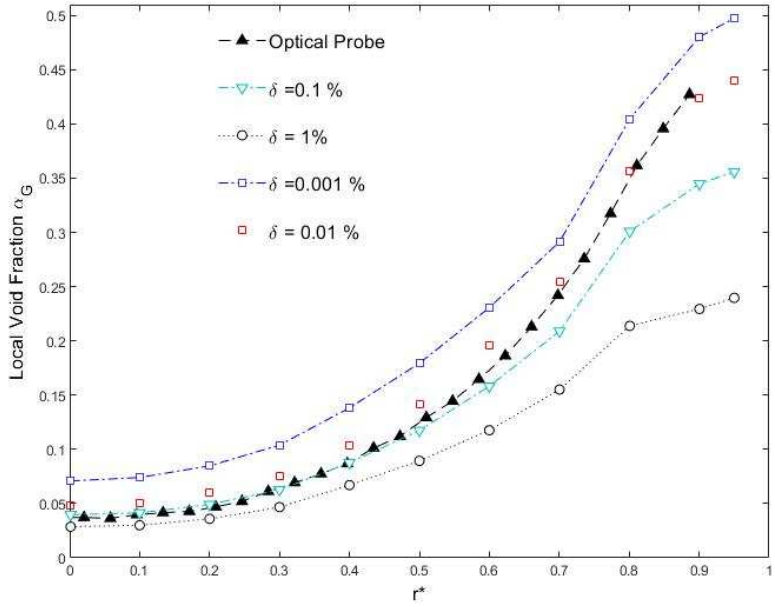

Figure 14: Comparison between the void fraction profiles measured with an optical probe and with the hot wire probes for several values of δ $a_w = 0.04$. Measurements have been performed with a Tungsten wire probe $d = 5\ \mu m$

A sensitivity analysis concerning the influence of the overheat ratio on the void fraction determination has also been performed (see Figure 15). It appears, as expected, that it is necessary to impose a high overheat, leading to boiling occurrence on the sensor's surface, in order to get an accurate value of the void fraction.

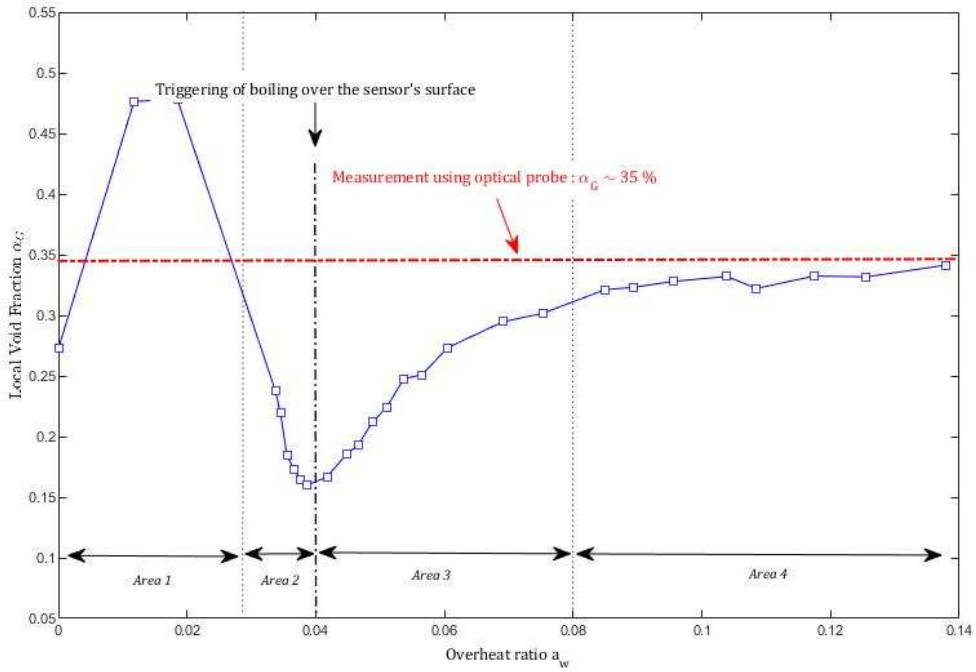

Figure 15. Influence of the overheat ratio on the void fraction determination using anemometry. Boiling occurs for $a_w = 0.04$

2.3.2 Liquid velocity and temperature measurements

We propose to use a methodology based upon the study of voltage distributions as suggested by Delhaye (1969). This author performed void fraction and liquid velocity measurements in an air/water flows using a hot-film probe operated in Constant Temperature Mode. He analyzed the sensor's voltage signal e_w in terms of voltage distribution and showed that the result can be seen as the superposition of two distributions, one being associated to the liquid phase, the other one characterizing the interaction between the gas and the sensor (hatched part on Figure 16).

Delhaye (1969) also indicated that the void fraction α_G was given by the ratio between the area of the gas part of the histogram (hatched part of the histogram $\mathcal{B}_{MNPQS}$ on Figure 16) and the whole area of the voltage distribution $\mathcal{B}_{tot}$. Once done, the voltage distribution corresponding to the liquid phase (corresponding to points Q, O and R on Figure 16) can be deduced.
This method has been used but adapted to our conditions, especially because the voltage distribution only reveal one peak, as shown on Figure 17 which can be explained by the interaction between the sensor and the gas phase (the bubbles size and the contact time between the probe and the bubble are so small that the sensor is not completely dried when in contact with the vapor).
To determine the voltage distribution corresponding to the liquid phase, we first determine the void fraction α_G, for a given set of thermal hydraulic conditions, using the procedure described in previous section. Then in the second step, we determine contribution corresponding to the vapor phase, which is approximated by the hatched part of the curve plotted on Figure 18.

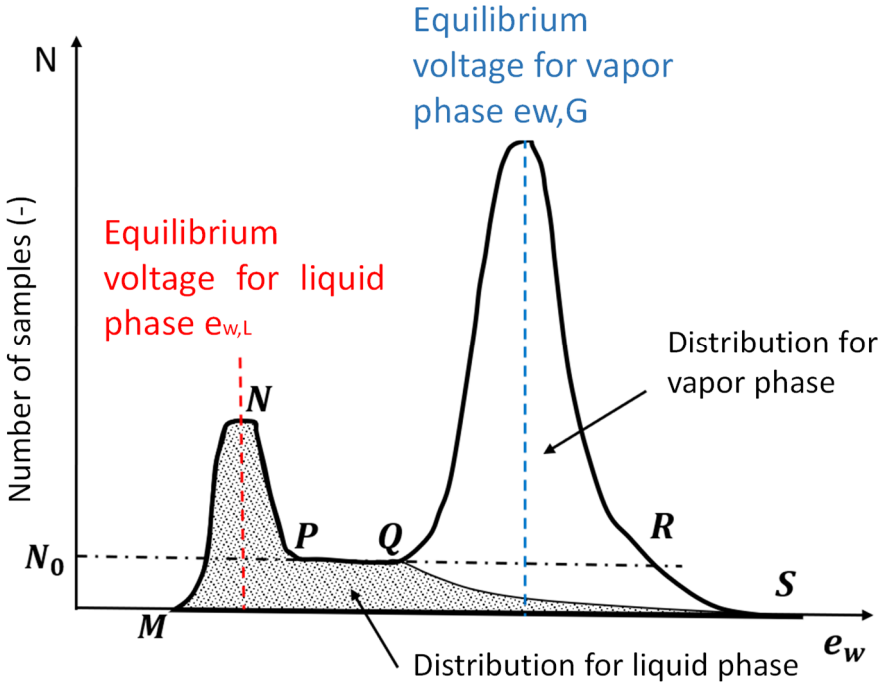

Figure 16. Typical sketch of corresponding voltage distribution. For CCA (Constant Current Anemometer), vapor distribution does correspond to higher values of voltage

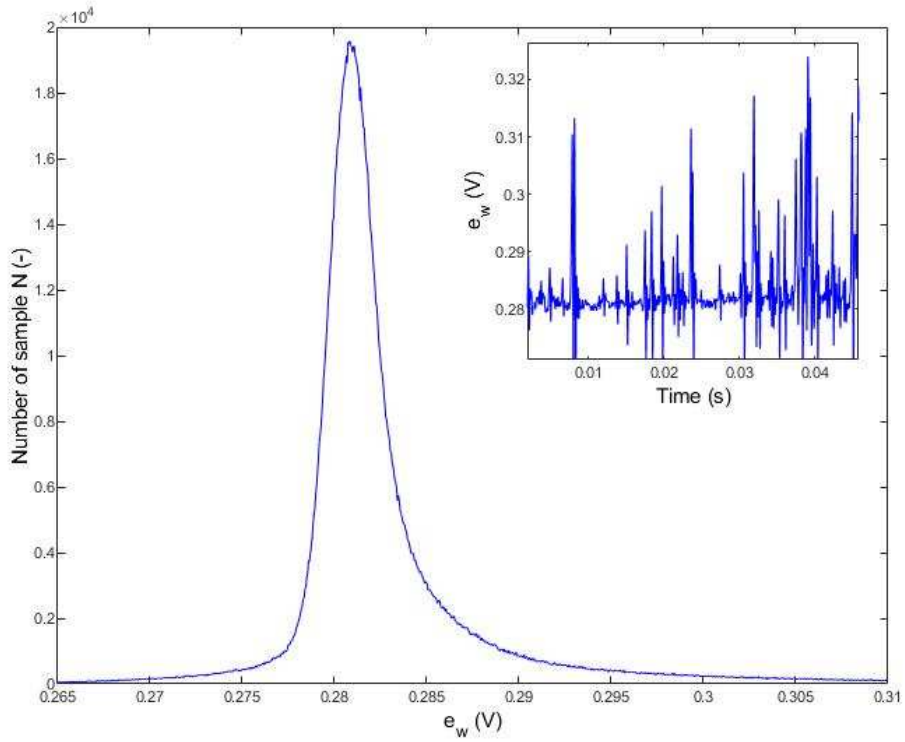

Figure 17: Typical voltage distribution

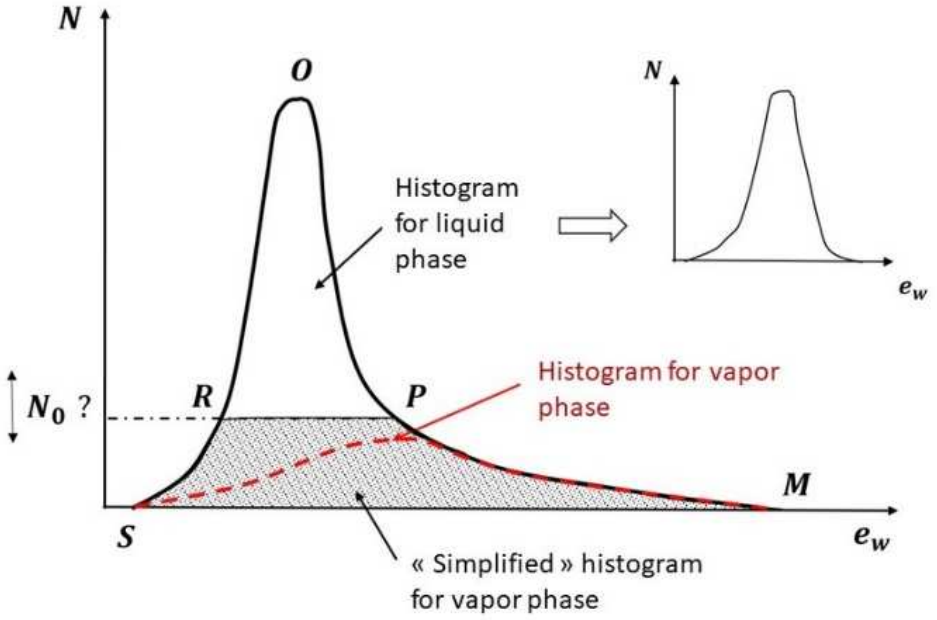

Figure 18: Determination of the voltage histogram which corresponds to vapor phase. The hatched curve corresponds to the approximated vapor histogram

The parameter N_0 is calculated according to the ratio between the areas $\mathcal{B}_{SRPM}$ and $\mathcal{B}_{SOM}$ where it is is equal to the void fraction α_G. Once done, we obtain the voltage distribution for the liquid phase ROP and the average value of the voltage corresponding to the liquid phase $e_{w,L}$ defined as:

$$e_{w,L} = \frac{\sum_{ROP} e_w\,(i)[N(i) - N_0]}{\sum_{ROP}[N(i) - N_0]} \tag{18}$$

The associated electrical resistance $R_{w,L}$ is defined as $R_{w,L} = e_{w,L}/I$. In similar manner to what has been done for the case of single-phase flow, we have plotted on Figure 19 the curve $R_{w,L}\left(R_{w,L}I^2/\lambda_f\right)$.

The red dotted line represents the curve which is obtained without any treatment. As we can see, this curve is no more linear. Such a behavior can easily be explained by the fact the heat transfer between the sensor and the surrounding fluid is no longer convective due to boiling occurrence on the surface of the wire. On the contrary, after the phasic discrimination procedure, which is represented by the black dotted curve appears to be linear. According to the multiple overheating method, this indicates a purely single-phase convective heat transfer. This result confirms the validity and the efficiency of the proposed methodology for the phasic discrimination. As previously, the liquid velocity can be deduced from the slope of this linear curve, whereas the liquid temperature corresponds to the intercept of the curve. Furthermore, we can notice that it is possible to directly access the liquid temperature without any phasic discrimination, since both curves (red and black) having the same intercept. The uncertainty of the velocity measurement is estimated to be 5%.

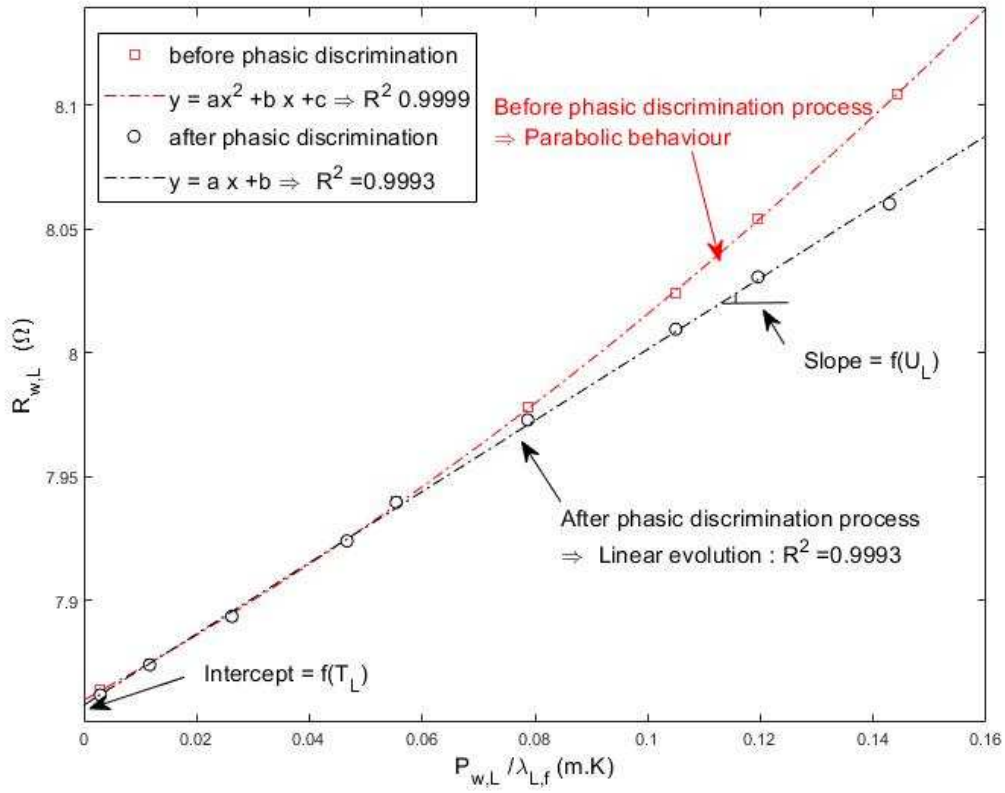

Figure 19. $R_{w,L}\left(R_{w,L}I^2/\lambda_f\right)$ after phasic discrimination ($r^* = 0.8$, $\alpha_G = 0.35$)

3 EXPERIMENTAL RESULTS

3.1 Single Phase Flows

The tests conditions are described in Table 3. Measurements have been performed with a hot-wire whose diameter is $5\ \mu m$. Data points were taken at 13 radial positions over one-half diameter. The overheat ratio a_w ranges from 0.14 to 0.2.

Run	P (bar)	G ($kg.m^{-2}.s^{-1}$)	T_{in} (°C)	q_p ($kW.m^{-2}$)	T_{out} (°C)
G3Q0	13.9	2998	20.0	0	20.0
G3Q20	13.9	2998	20.0	21.0	23.4
G3Q40	13.9	2995	20.1	39.4	26.6
G3Q60	13.9	2999	20.0	59.9	29.9
G3Q80	13.9	3000	20.1	81	33.7

Table 3 : Experimental conditions of the R134A DEBORA data base for heated single-phase flows

Run G3Q0 aimed to check the assumption of axis symmetry of the flow. As we can see on Figure 20, the axis-symmetry of the flow seems to be good according to the uncertainties.
Figure 21 and Figure 22 display the non-dimensional liquid velocity and temperature profiles for the tests described in Table 3. We also have plotted the theoretical liquid velocity and temperature profiles obtained using the model of Deissler (1963) coupled with the Prandtl's analogy assumption on the same figure. In our experiments, the nearest measurement position is located at 0.3 mm from the wall.

We can notice that there is a good agreement between the experimental results and the theoretical profiles. In addition, mass and energy balances have been checked and are less than $3\ \%$ and $0.2\ °C$ respectively. Some turbulent fluctuations measurements have also been performed for adiabatic flows at a pressure of $26\ bar$ and a mass flux of $1000\ kg.m^{-2}s^{-1}$.

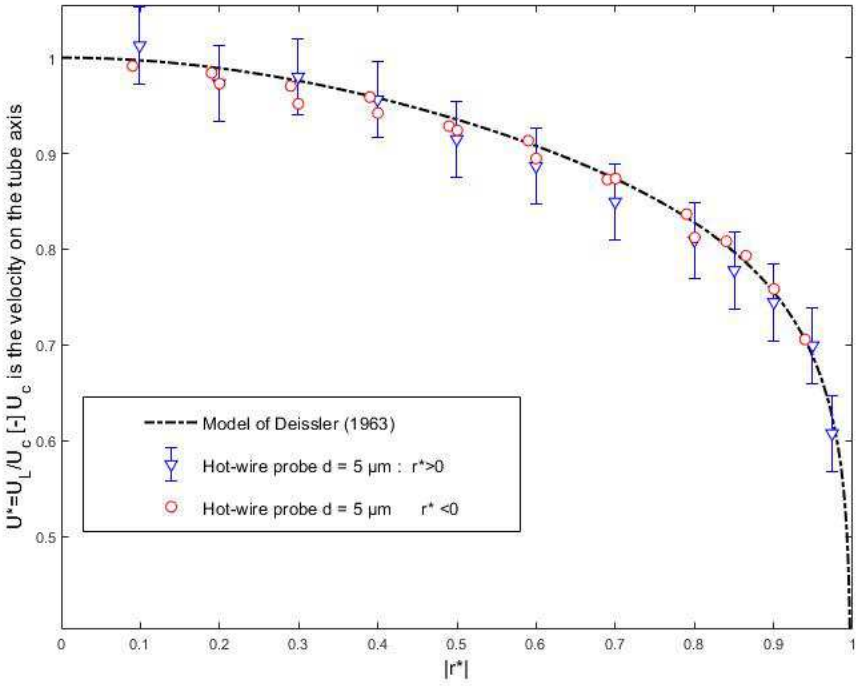

Figure 20 : Liquid velocity radial profile for Run G3Q0. U_C is the velocity on the axis of the tube.

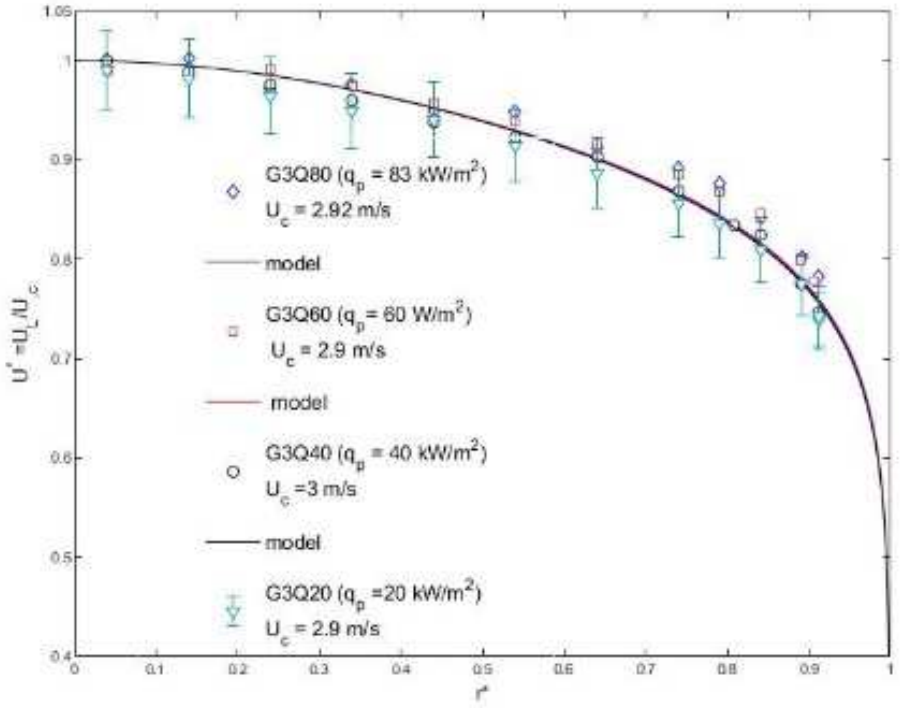

Figure 21: Liquid velocity profile U_C is the velocity on the axis of the tube.

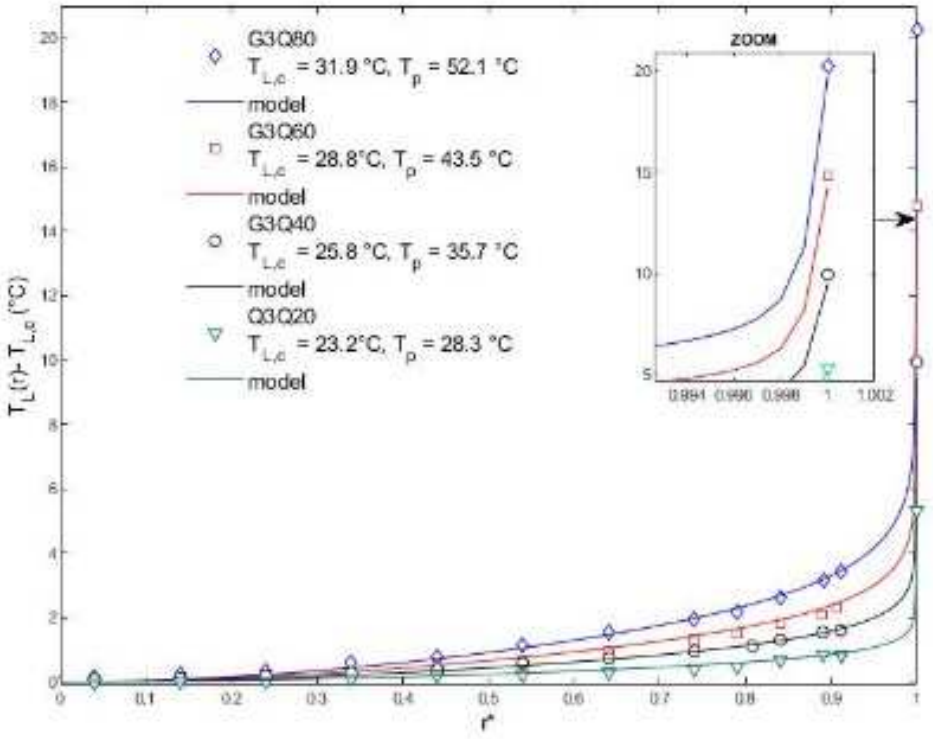

Figure 22: Liquid temperature profile T_{LC} is the temperature on the axis of the tube

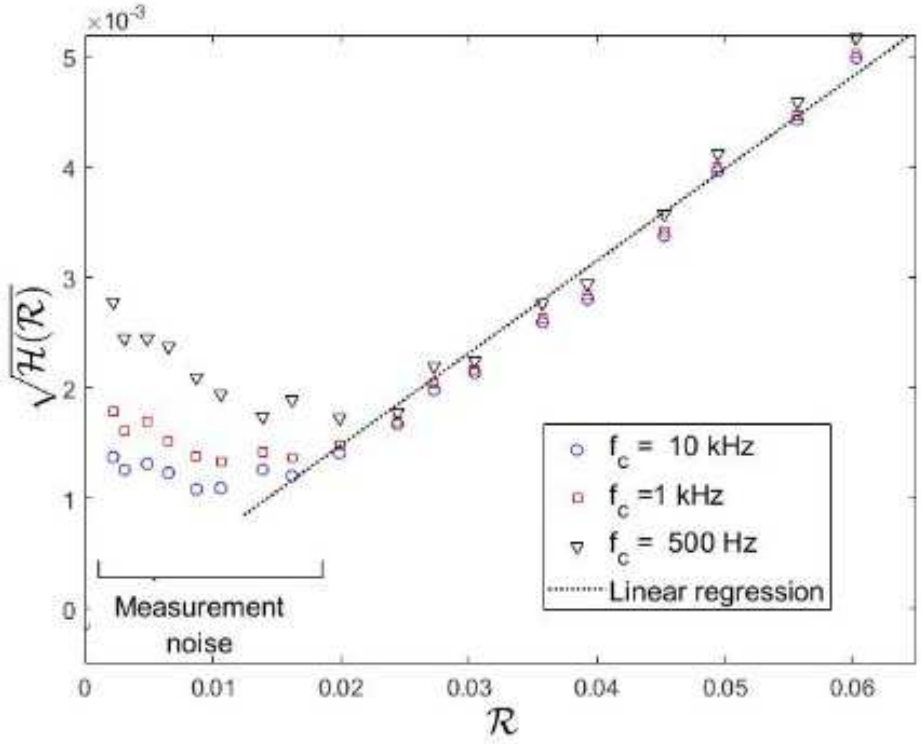

Figure 23: Fluctuation diagram for different values of the compensation frequencies. The probe is located at $r^* = 0.9$

The results are plotted on Figure 23. For $\mathcal{R}>0.02$, we can observe a linear behavior as predicted by equation 17 for adiabatic configuration, where no temperature fluctuations are expected. In addition, we can also notice that the slope seems to be weakly affected by the cutoff frequency. This probably indicates that most of the energy is at large scales, *i.e.* low frequencies within the energy spectra. On the other hand, for low values of $\mathcal{R}$ (which corresponds to low overheat), the experimental data deviate from the linear behavior, which has no physical soundness but can be explained by a too low signal-to-noise ratio.

3.2 Boiling flows

Five tests have been performed (see Table 4) using a hot-wire probe whose diameter is $d = 5\mu m$ and length is $l = 700\,\mu m$. Those tests have been performed in two steps: (i) first, void fraction measurements then (ii) liquid and temperature measurements.

Run	P (bar)	G ($kg.m^{-2}.s^{-1}$)	T_{in} (°C)	q_p ($kW.m^{-2}$)
Q200Te29	14.6	2780	29.0	203
Q140Te37	14.6	2780	37.0	141
Q110Te41	14.6	2780	41.0	112
Q81Te45	14.6	2780	45.0	81
Q48Te48	14.6	2780	48.0	48

Table 4. Experimental conditions of the R134A DEBORA data base for boiling flows

For those conditions, void fractions and liquid temperature have also been measured with an optical probe and a thermocouple whose diameter was 250 µm. Figure 24 and Figure 25 show the

comparison between the experimental results performed with anemometry and those obtained using the technics previously mentioned. The parameter δ is set to 10^{-4} as recommended before. We can see that there is a very good agreement between both kinds of instrumentation for void fraction as well as for temperature measurements. Concerning the void fraction, the maximum deviation is $5\ \%$ which is consistent with the uncertainty of the optical probe that is estimated to be close to 2%. Those differences may be explained by a spatial filtering effect of the wire sensor due to its length ($l \sim 700\ \mu m$) which is larger than the characteristic size of the optical probe ($l \sim 10\ \mu m$).
Concerning the liquid temperature profiles, the maximum deviation is $0.5\ °C$, which is consistent with the uncertainty of the thermocouples, since they have been carefully calibrated. Those results confirm the accuracy of the measurements performed by thermocouples even if those measurements have been performed without any phasic discrimination procedure.

Figure 26 and Figure 27 display the liquid and the vapor velocity profiles measured by both anemometry and optical probes. We observe that the liquid velocity increases with the heat flux. In the same time, the profiles are flattening. This behavior results from the void fraction increasing which implies a fluid acceleration. The velocity increase also induces an enhancement of the turbulent mixing which also tends to flatten the profiles. We can notice a very similar behavior for the vapor velocity profiles. We can also see that the relative velocity between the vapor and the liquid seems to be constant in the core but tends to increase as we get closer to the heated wall for high heat fluxes. This indicates that it will probably be necessary to consider for mechanical non-equilibrium conditions to describe the flow behavior in the vicinity of the wall.

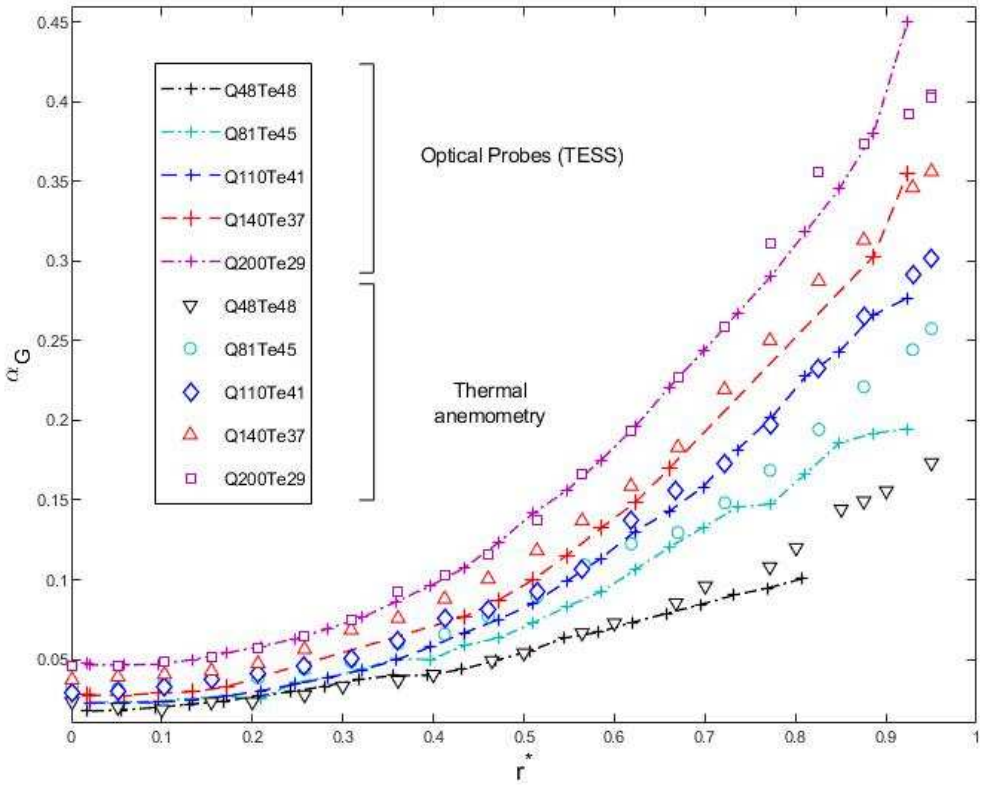

Figure 24: Comparison between void fraction profiles measured by anemometry and optical probe

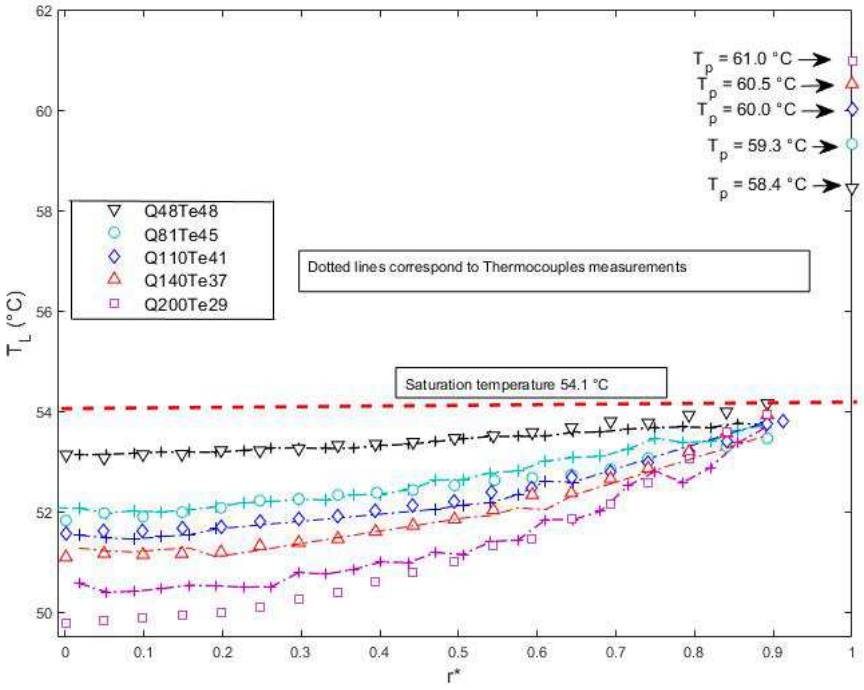

Figure 25: Comparison between liquid temperature measurements performed with anemometry and thermocouples

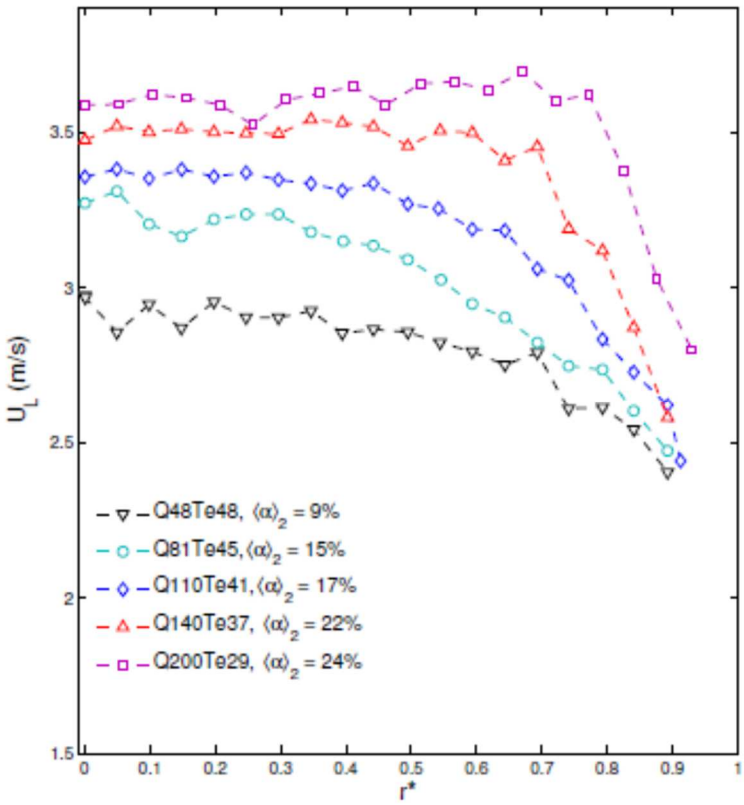

Figure 26: Liquid velocity profiles measured by anemometry

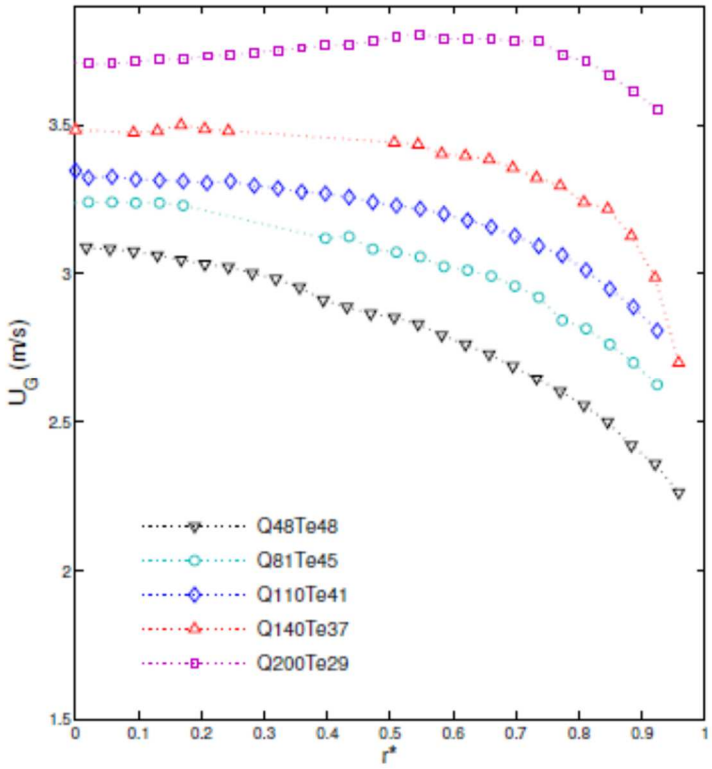

Figure 27: Vapor velocity profiles measured by optical probes

4 CONCLUSIONS

In this paper, we have proposed a methodology for measuring the liquid velocity, temperature and void fraction profiles within a Freon R134A boiling flow using thermal anemometry. We use the multiple overheating method whose application for liquid is innovative. To overcome the influence of liquid temperature on velocity calibration, we proposed a new dimensionless representation of the calibration curve. Using the fluctuation diagram, it has been possible to access the velocity fluctuations for single phase flows. Concerning boiling flows, a two-steps approach has been used. The void fraction is measured first with boiling over the surface of the sensor. The liquid velocity and temperature are then measured using the voltage histogram method. Furthermore, the liquid temperature may be accessed with a good accuracy without any phasic discrimination procedure.

Some perspectives can be listed for going on this work. First concerns the maximum overheat that can be achieved on the surface of the sensor. This limitation prevents getting accurate measurements from the velocity fluctuations. A possible idea would be to deposit a smoothing coating on the sensor to fill the cavities on its surface who act as nucleation sites. DLC (Diamond Like Carbon) could be a good candidate. Another prospect would concern the enhancement of the signal-to-noise ratio at low overheat to perform more accurate measurements of the liquid temperature fluctuations. Finally, it could also be interesting to develop a sensor made of several wires to measure the vapor velocity by cross-correlation.

5 REFERENCES

1. Arwatz G., Bahri C., Smits A. J., Hultmark M., Dynamic calibration and modeling of a cold wire for temperature measurement, *Measurement Science and Technology*, **Vol.** 24, 2013

2. Comte-Bellot G., Hot wire anemometry, *Annual Review of Fluid Mechanics*, **Vol.** 8, pp. 209-231, 1976
3. Corrsin S., Extended applications to the hot-wire anemometer, *Review of Scientific Instruments*, **Vol.** 18, 1947
4. Deissler R. G., Turbulent heat transfer and temperature fluctuations with uniform velocity and temperature gradients*, Int. Journal of Heat and Mass Trans.*, **Vol.**6, 1963,
5. Delhaye J.-M. D., Hot-film anemometry in two-phase flows, *Proc. 11th Nat. ASME/AIChe Heat Trans. Conf. on Two-Phase Flow Instrumentation*, pp. 523-509, 1969
6. Dix G., *Vapor void fractions for forced convection with subcooled boiling at low flow rates*, Ph. D. Thesis, University of California, 1971
7. Farrar B., Samways A. L., Bruun H. H., A computer-based hot-film technique for two-phase flow measurements, *Meas. Sci. Tech.*, **vol.** 6, 1995
8. Kramers H., Heat transfer from spheres to flowing media, Physica, **Vol. 12**, 1946
9. Liu T. J., Bankoff S. G., Structure of air-water bubbly flow in a vertical pipe (i) liquid mean velocity and turbulent measurements, *Int. Journal of Heat and Mass Trans.*, **Vol. 36**, 1991
10. Morkovin M. V., Fluctuations and hot-wire anemometry in compressible flows*, Report from Advisory Group for Aerospace Research and Development (NATO)*, 1956
11. Stevens G. F., Kirby G. J., A quantitative comparison between burnout data for water at 1000 psia and freon-12 at 155 psia uniformly heated round tubes, vertical up-flow, *United Kingdom Atomic Energy Authority, Report Number AEEW-R327*, 1964
12. Tagawa M., Shimoji T., Ohta Y., A two-thermocouples technique for estimating thermocouple time constant in flow with combustion: In situ parameter identification of a first-order lag system, *Review of Scientific Instruments*, **Vol.** 69, n°9, 1998,
13. Zagarola M.V., Smits A.J., Mean-flow scaling of turbulent pipe flow*, Journal of Fluid Mechanics*, **Vol.** 373, 1998
14. Albrecht H., Borys M., Damaschke N., Tropea C., Laser Doppler and Phase Doppler Measurement Techniques, Springer Verlag, 2003
15. Charonko J.J., Prestridge K., Variable-density mixing in turbulent jets with coflow, *Journal of Fluid Mechanics*, Vol. 825, 2017, pp. 887-921
16. Pope S.B., Turbulent Flows, Cambridge University Press, 2000
17. Garnier J., Manon E., Cubizolles G., Local measurements on flow boiling of refrigerant 12 in a vertical tube, Multiphase Science and Technology**, Vol.** 13, 2001, pp. 1-111
18. Bruun H.H., Hot-wire anemometry, Oxford University Press, 1995

6 Appendix

The experimental set-up is described in Figure 28. Operated under constant current mode (CCA), the circuit is mainly made of:

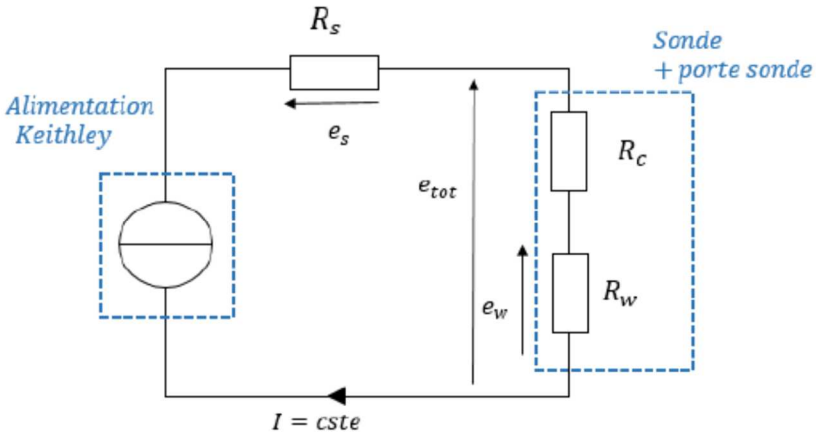

Figure 28 : Description of the measurement circuit

- The sensor, which includes the wire-probe whose electrical resistance is R_w and its connecting device whose electrical resistance is R_C. The connecting device is composed of the prongs whose electrical resistance R_p is given by the probe manufacturer ($R_p = 0.5\ \Omega$) and the receiving apparatus whose electrical resistance R_{Ra} is measured using a short-circuit resistance ($R_{Ra} = 0.4\ \Omega$). The probe is manufactured by DANTEC ® (model 55P11).
- A regulated power supply (Keithley® 2450) which is able to supply current up to 1A for a voltage of 21V.
- A Shunt resistor ($R_s = 10\ \Omega$) which is used by Kledy to accurately measure the current which is delivered by the power supply by measuring the voltage at its terminals.
- An acquisition board. Kledy used a National Instrument NI6259 including 32 analog input channel and whose resolution is 16 bit to get a digitalization as accurate as possible. The maximum sampling frequency is 300 KHz for all the input channels. During the tests, the sampling frequency is 60 kHz.

Two additional devices are included in the circuit:

- a band pass filter whose cutoff frequencies are $f = 50\ Hz$ and $f = 10\ kHz$ to eliminate both low-frequency voltage fluctuations below 50 Hz and high frequency noise above 10 kHz
- A measurement amplifier whose gain can adjusted between 20 and 80 dB. This device is interesting when measuring the voltage fluctuations at the wire terminals. This is specifically useful if you aim to perform turbulence measurements or if you operate under boiling flows to make the distinct between liquid and vapor phase, which is closely linked to the voltage fluctuations at the sensor's terminals.

Table 5 sums up the main characteristic of the devices included in the whole measurement chain.

Device	Range	Accuracy	Resolution
Acquisition board NI 6259	-10 V / +10 V -5V / +5V -2V / +2V -1V / +1V -0.5V / +0.5V	± 1.92 mV ± 1.01 mV ± 410 µV ± 220 µV ± 130 µV	± 52 µV ± 56 µV ± 13 µV ± 13 µV ± 8 µV

	-0.2V / +0.2V -0.1V / +0.1V	± 74 µV ± 52 µV	± 6 µV ± 6 µV
Power supply Keithley 2450	1 mA / 10 mA 10 mA / 100 mA 100 mA / 1 A	0.02% + 1.5 µA 0.025% + 15 µA 0.0067% + 900 µA	500 nA 5 µA 50 µA
Measurement Amplifier DLPVA 100-FD	±10 V	0.1%	[-]
Shunt Resistor	10 Ω	0.01%	[-]

Table 5: Characteristic of the measurement chain